Space Sci Rev (2017) 213:205–218
DOI 10.1007/s11214-017-0428-7

The Juno Gravity Science Instrument

Sami W. Asmar[1] · Scott J. Bolton[2] · Dustin R. Buccino[1] · Timothy P. Cornish[1] · William M. Folkner[1] · Roberto Formaro[3] · Luciano Iess[4] · Andre P. Jongeling[1] · Dorothy K. Lewis[1] · Anthony P. Mittskus[1] · Ryan Mukai[1] · Lorenzo Simone[5]

Received: 4 May 2017 / Accepted: 4 October 2017 / Published online: 25 October 2017

Abstract The Juno mission's primary science objectives include the investigation of Jupiter interior structure via the determination of its gravitational field. Juno will provide more accurate determination of Jupiter's gravity harmonics that will provide new constraints on interior structure models. Juno will also measure the gravitational response from tides raised on Jupiter by Galilean satellites. This is accomplished by utilizing Gravity Science instrumentation to support measurements of the Doppler shift of the Juno radio signal by NASA's Deep Space Network at two radio frequencies. The Doppler data measure the changes in

✉ W.M. Folkner
william.m.folkner@jpl.nasa.gov

S.W. Asmar
Sami.W.Asmar@jpl.nasa.gov

S.J. Bolton
sbolton@swri.edu

D.R. Buccino
Dustin.R.Buccino@jpl.nasa.gov

T.P. Cornish
Timothy.P.Cornish@jpl.nasa.gov

R. Formaro
Roberto.Formaro@asi.it

L. Iess
Luciano.Iess@uniroma1.it

A.P. Jongeling
andre.p.jongeling@jpl.nasa.gov

D.K. Lewis
dorothy.k.lewis@jpl.nasa.gov

A.P. Mittskus
Anthony.P.Mittskus@jpl.nasa.gov

R. Mukai
Ryan.Mukai@jpl.nasa.gov

L. Simone
Lorenzo.Simone@thalesaleniaspace.com

the spacecraft velocity in the direction to Earth caused by the Jupiter gravity field. Doppler measurements at X-band (∼ 8 GHz) are supported by the spacecraft telecommunications subsystem for command and telemetry and are used for spacecraft navigation as well as Gravity Science. The spacecraft also includes a Ka-band (∼ 32 GHz) translator and amplifier specifically for the Gravity Science investigation contributed by the Italian Space Agency. The use of two radio frequencies allows for improved accuracy by removal of noise due to charged particles along the radio signal path.

Keywords Gravity field · Radio systems

1 Introduction and Science Objectives

An overview of the Juno mission is provided by Bolton et al. (2017). The objective of the Juno Gravity Science experiment is to estimate the gravity field of Jupiter in order to provide constraints on models of the interior structure. Since the motion of the Juno spacecraft is perturbed by the gravity field of Jupiter, one can recover the gravity field by accurately tracking the motion of the spacecraft. Prior to the arrival of Juno, the gravity field of Jupiter was estimated from the Doppler measurements acquired by the Pioneer 10 and 11 (Anderson et al. 1974; Null et al. 1975), the Voyager 1 and 2 spacecraft (Campbell and Synnott 1985) and the Galileo spacecraft (Jacobson et al. 1999; Jacobson 2003, 2009). These data provided estimates of the low-degree spherical harmonic coefficients as well as the mass and spin-pole direction of Jupiter. These estimates have been used to constrain Jupiter interior models but leave significant parameters, such as the existence of, and mass of, a core of elements heavier than hydrogen and helium (e.g. Nettelmann et al. 2012; Miguel et al. 2016; Hubbard and Militzer 2016).

Juno will enable a more accurate determination of the Jupiter gravity harmonics because of more favorable orbital geometry and more accurate Doppler measurements than previous missions. If Jupiter has a dense core of heavy elements (elements other than hydrogen and helium), gravity harmonics will set constraints on the mass and radius of the core. If there is no central core, the gravity harmonics will constrain the radius of the central region in which heavy elements are mixed with the hydrogen and helium. Juno may reveal the possibility of gravity field due to differential rotation that may appear as increased values of higher-order zonal harmonics and/or as measureable values of odd zonal harmonics (Kaspi 2013). Juno will also measure the gravitational response from tides raised on Jupiter by Galilean satellites that may provide additional constraints on the Jupiter interior structure (Wahl et al. 2016).

The Juno trajectory was designed to provide 32 polar orbits of Jupiter with an 11-day orbital period. These provide sampling of the magnetic field every 11.25° of longitude. Most of the early orbits were intended primarily for the Microwave Radiometer (MWR) (Janssen et al. 2017) while most of the later orbits were intended for the Gravity Science experiment.

1 Jet Propulsion Laboratory, California Institute of Technology, Pasadena, CA, USA

2 Southwest Research Institute Space, San Antonio, TX, USA

3 Italian Space Agency, Rome, Italy

4 Dipartimento di Ingegneria Aerospaziale ed Astronautica, Università La Sapienza, Rome, Italy

5 Thales Alenia Space-Italy, 00131 Rome, Italy

The 32 orbits were planned to be completed in less than one year so that solar conjunction would not occur during the science phase.

The Gravity Science instrumentation was developed to achieve Doppler measurement accuracy comparable to the best previously achieved accuracy by the Cassini radio science experiment (Kliore et al. 2004) for the 11-day orbit mission plan. In order to achieve this accuracy, two coherent radio links are used. The X-band link utilizes a signal transmitted by a Deep Space Network (DSN) tracking station at ~ 7.2 GHz and detected at the spacecraft, which multiples the signal by a fixed integer ratio and transmits to Earth a frequency ~ 8.4 GHz. For the Ka-band link the DSN station transmits a signal frequency ~ 34 GHz that the spacecraft detects, multiples by a fixed integer ratio, and transmits back to Earth at ~ 32 GHz. The use of two radio frequencies allows cancellation of most of the noise of the Doppler measurement due to charged particles along the signal path between the station and the spacecraft (Mariotti and Tortora 2013). This cancellation is expected to reduce the noise due to charged particles to below the residual noise due to Earth troposphere fluctuations as long as the angular separation of Jupiter and the Sun as seen from Earth is greater than 15°.

After arrival at Jupiter the trajectory plan was changed to use a spacecraft orbital period of 53-days. A total of 32 science orbits are still planned. The 53-day orbits provide more accurate gravity science since the angle between the normal to the orbit and the direction from Jupiter to Earth is, on average, larger with the 53-day orbits. This larger angle results in a larger projection of the changes in spacecraft velocity due to the gravity field onto the Jupiter–Earth direction and a larger measured signal in the Doppler data.

Section 2 gives an overview of the Gravity Science instrumentation. Sections 3 and 4 give more details on the instrumentation on the spacecraft and at the DSN station. Section 5 gives a brief assessment of expected Doppler measurement accuracy.

2 Measurement Process & Instrumentation Overview

The precision Doppler measurement process is based on the carefully designed dual-band instrumentation represented in Fig. 1. The transmitted signal frequencies and integer ratios used at the spacecraft to multiply the received frequency from Earth before transmission are given in Table 1.

The observed Doppler shift is the difference between the signal frequency from the spacecraft received at the DSN station and the frequency transmitted by the DSN station one round-trip light-time earlier multiplied by the spacecraft re-transmission (transponder) ratio. In practice, the DSN tracking station records the transmitted frequencies and the received frequencies as a function of time referenced to the highly-stable hydrogen maser station frequency reference (Lauf et al. 2005). The Doppler shift is then computed using light-time iteration algorithms (Moyer 2000).

The X-band transmission from the station is also used to send commands to the spacecraft and the X-band transmission from the spacecraft used to send telemetry data from the Juno science instruments and engineering sub-systems to Earth. The Doppler shift of the X-band carrier frequency is used for spacecraft navigation (e.g. Thompson et al. 2014) as well as for gravity science. The Ka-band equipment is used to provide improved Doppler accuracy specifically for Gravity Science. Mukai et al. (2012) provide more details on the Juno telecommunications subsystem.

Only one DSN tracking station, with designation DSS-25 at Goldstone, California has the capability of transmitting the Ka-band signal to the spacecraft. The Juno trajectory was originally designed so that all close flybys of Jupiter (perijoves) take place within view of

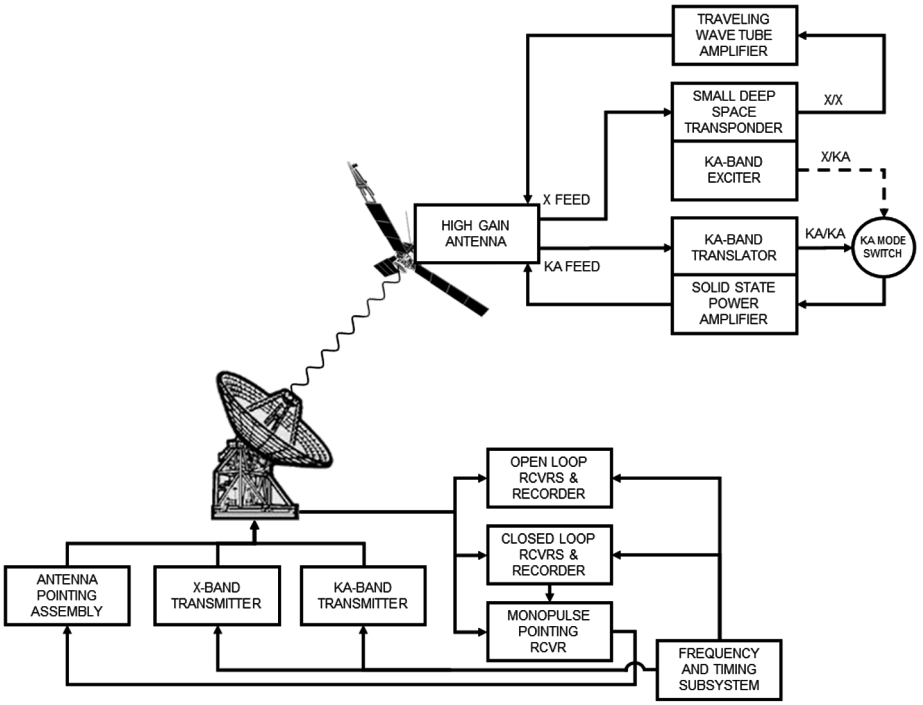

Fig. 1 Block diagram of the Juno gravity science instrumentation on the Juno spacecraft and at the Deep Space Network tracking station in Goldstone, California

Table 1 Frequencies for radio links on Juno

Band (uplink/ downlink)	Uplink frequency range (MHz)	Downlink frequency range (MHz)	Transponder ratio (downlink/uplink)
X/X	7153	8404	880/749
Ka/Ka	34367	32085	3360/3599
X/Ka	7153	32088	3360/749

DSS-25. After launch, one additional perijove was inserted at the start of science operations not in view of DSS-25; Doppler data with only X-band uplink can be acquired from the DSN tracking stations in Madrid, Spain. The change in the orbit period after arrival at Jupiter also accommodated tracking at DSS-25 for all perijoves except the additional perijove at the start of science operations.

At perijoves, the Juno spacecraft attitude is optimized either for Gravity Science or for MWR observation. For the former, the spacecraft high-gain antenna (HGA) along the spacecraft spin axis is pointed towards Earth. For MWR observation, gravity measurements are not planned since the spacecraft spin axis is pointed perpendicular to the orbit plane to optimize view of Jupiter by the MWR antennas on the sides of the spacecraft perpendicular to the spin axis; the Earth will not be within the beamwidth of the HGA.

During Gravity Science perijoves, DSS-25 transmits signals at X-band and Ka-band to the spacecraft with frequencies referenced to the DSN high-precision clock. These signals

are received by the spacecraft HGA. The X-band signal is fed to the Small Deep Space Transponder (SDST) that detects the carrier signal and generates a coherent frequency for transmission to Earth by multiplying the received frequency by the ratio shown in Table 1. The X-band transmission frequency output from the SDST is amplified by a traveling-wave-tube amplifier (TWTA) and transmitted by the HGA. The Ka-band signal from DSS-25 is fed to the Ka-band Translator (KaT) that detects the carrier frequency and multiples by the ratio of integers given in Table 1 for transmission back to Earth. The KaT output signal is amplified by a solid-state power amplifier (SSPA) and transmitted to Earth though the HGA.

When no Ka-band signal uplink is available from Earth, as in the first science perijove, the SDST generates a Ka-band downlink based on the X-band uplink in addition to the primary X-band downlink signal. This Ka-band signal is then amplified by the SSPA and transmitted by the HGA and is useful for providing partial calibration of the effect of charged particles on the Doppler measurement.

3 Flight Instrument Elements

Although the dynamic behavior of the entire spacecraft affects the quality of the Doppler observable and the Gravity Science investigation, this section focuses on the telecommunications transponder, the Ka-band Translator and their power amplifiers as well as Juno's high-gain antenna (HGA).

3.1 Small Deep Space Transponder and Power Amplifier

The Juno telecommunications subsystem is described in Mukai et al. (2012) and Fig. 1 shows a block diagram of its functional aspects. The subsystem is centered on two redundant, but not identical, Small Deep Space Transponders (SDST) with very high flight heritage. This transponder has a nominal assigned frequency as shown in Table 1 along with the standard X-band turn-around ratio. It is used for command and telemetry communications as well as radio-metric tracking to produce Doppler and ranging observables for navigation. The X-band Doppler data are also used for Gravity Science during the designated perijove flybys described above.

One Juno SDST is the prime unit and operates at X/X/Ka, short for X-band uplink and X-band as well as Ka-band downlink, both coherent with the X-band uplink. The second or back-up SDST operates at X/X, which is X-band uplink and downlink. The difference between the two transponders is a "times 4 multiplier" present in the prime unit that converts a copy of the output X-band frequency to Ka-band downlink—different from the output of the Ka-band Translator discussed below. However, the output of the SDST utilizes the amplifier in the Ka-band Translator to amplify the output RF signal for transmission. Figure 2 shows the Juno SDST and its four modules: Exciter, Down Converter Module (DCM), Digital Processor Module (DPM), and Power Converter Module (PCM). The two SDST output frequencies to the exciters are labeled 880 F1, which is the X/X configuration described above, and 840 F1, which drives an external X4 multiplier to generate a Ka-band signal. F1 is determined exactly by the assigned DSN channel and is ~ 9.5 MHz.

The X-band signal generated by the transponder is amplified via redundant X-Band traveling wave tube amplifiers (TWTAs) procured from Tesat/Thales. Each TWTA output power is 25 W with required DC input power of 56 W. The TWTA is comprised of the traveling wave tube, which is the RF amplifying element, and an electronic power converter.

Fig. 2 The Juno Small Deep Space Transponder showing the four modules

3.2 Ka-band Translator and Power Amplifier

The Ka-band Translator (abbreviated KaT or KaTS in some documentation when viewed along with its accompanying Ka-band power amplifier as a subsystem) is functionally a Ka-band to Ka-band transponder used for Gravity Science Doppler tracking. It is referred to as a translator rather than a transponder because it processes the carrier-only signal without any modulation on either the uplink input to the KaT or downlink output of the KaT. A notable difference between the KaT and the SDST described above is that the KaT is classified as a science-class instrument and is not redundant while the SDST is a critical spacecraft element and is redundant. The KaT is contributed to Juno by the Italian Space agency (ASI) and built by Thales Alenia Space-Italy (TAS-I) company near Rome, Italy. The translator receives a Ka-band uplink carrier from one DSN station (currently only DSS-25 has the capability to transmit at Ka-band) at 34 GHz and returns a coherent frequency-translated downlink carrier at 32 GHz, amplified to output power of 2.5 W, or 34.5 dBm. The turn-around ratio is shown in Table 1.

Ciarcia et al. (2013) describe the Juno KaT as having four functional modules: a receiver analog module, a digital module, a transmitter analog module, and a baseplate module; see Fig. 3. The first step in the receiver module is low-noise amplification, with the amplifier placed as a hybrid outside the KaT box. This is followed by down-converting the RF signal to intermediate-frequency (IF). The IF signal is then digitized by an analog-to-digital converter where a wide-band automatic gain control, controlled by the field-programmable gate array (FPGA) integrated circuit, keeps the input power constant.

With the signal represented by digital samples, the key follow-up operations are handled by the RTAX2000S FPGA at the core of the digital module. It further down-converts the digital samples from IF to baseband In-Phase and Quadrature (I and Q) signals, processes the critical coherent turn-around conversion, and carries out the direct digital synthesis (DDS) functions for the uplink carrier tracking, based on a third-order phase-locked loop, as well as the downlink signal generation. Ciarcia et al. (2013) includes a detailed block diagram of these operations.

The transmitter analog module uses a phase-locked loop function to set the down-link frequency to the desired value. The loop's output is followed by a frequency multiplier of a factor of four in the form of two cascaded $\times 2$ multipliers. The final step is power amplification of the output, which is performed by the Ka-band solid-state power amplifier

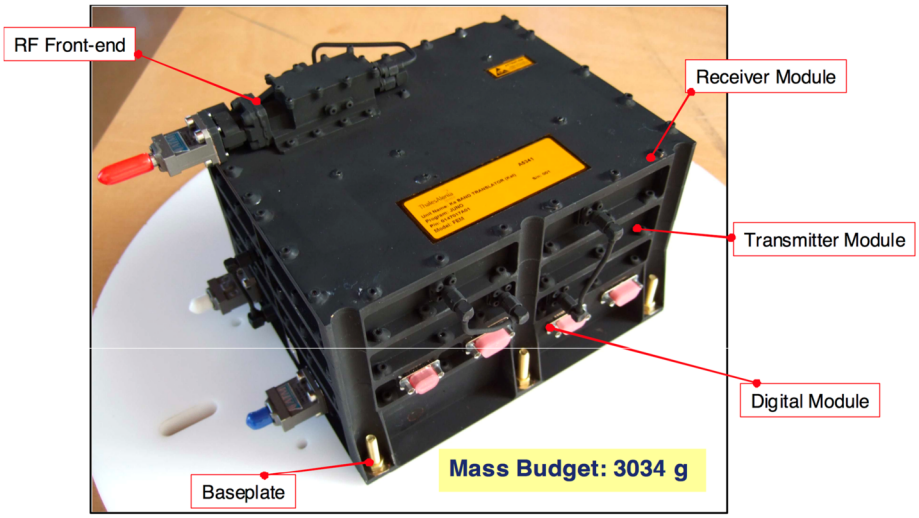

Fig. 3 A picture of the Juno Ka-Band Translator from the manufacturer showing the four functions modules described above and the low-noise amplifier in the RF front-end on top (source: Ciarcia et al. 2013)

(SSPA). The 2.5 W SSPA is integrated in the KaT's baseplate module which also includes two DC/DC converters for maximizing the power efficiency.

3.3 High Gain Antenna

Juno has five antennas for communications purposes. The Gravity Science investigation primarily utilizes the high-gain antenna (HGA), which is a 2.5 m diameter dual-band (X- and Ka-bands) dual reflector antenna. Specific gain performance and relevant parameters are listed in Mukai et al. (2012). Vacchione et al. (2012) describe how the HGA diameter selection was limited to 2.5 m by the spacecraft packaging and the size of the shroud in the Atlas V launch vehicle. The arrangement of the large three-armed solar array of the spinning spacecraft limited the spacecraft attitude control that point the HGA's main beam to approximately $+/-0.25$ degrees. They further describe how the required gain at X-band of 41.4 dBi to 43 dBi (for uplink and downlink respectively) was readily achievable with a 2.5 m diameter aperture.

After maximizing the antenna performance at X-band, the design team successfully addressed the challenge of adjusting the Ka-band beamwidth to match that of the X-band radiation pattern. They proposed a dual-reflector Gregorian style optics consisting of a parabolic main dish and an elliptical subreflector; a dual X/Ka-band feed had already been developed. Vacchione et al. (2012) describe the details of the final design that modified the Ka-band radiation pattern such that its gain and beamwidth matched the X-band gain and beamwidth without appreciably impacting the X-band performance. The Ka-band shaped pattern resulted in a flattened beam top with the desired properties.

The reflectors were fabricated by ATK Space Systems and a radome was added over the HGA for thermal control and meeting the temperature extremes over the life of the mission. Figure 4 shows the location of antennas on the Juno spacecraft and Fig. 5 shows the HGA with the radome thermal blanket as it was being installed on the spacecraft bus shortly before launch, as well as the relative sizes.

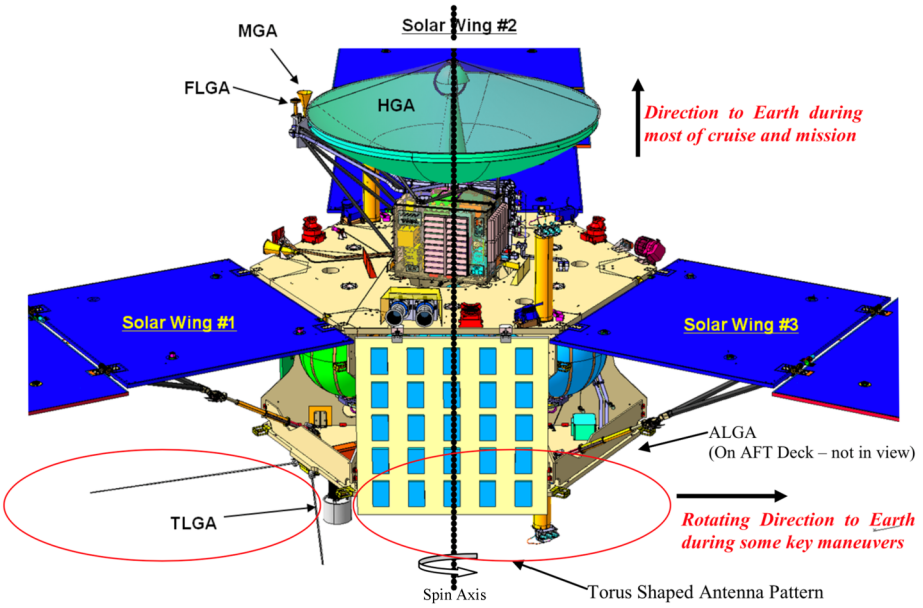

Fig. 4 The location of antennas on the Juno spacecraft

Fig. 5 The location of antennas on the Juno spacecraft

The antenna patterns can be found in Mukai et al. (2012) and Vacchione et al. (2012). The HGA has a right-hand circular polarization (RHCP) at X-band for uplink and downlink. It has RHCP at Ka-band for downlink and left-hand circular polarization (LHCP) for Ka-band uplink.

4 Ground Instrument Elements

NASA's Deep Space Network (DSN) consists of three complexes that provide communications with spacecraft throughout the Solar System. They are located at Goldstone, California, Madrid Spain, and Canberra, Australia, equally-spaced in longitude to provide continuous coverage when needed. Each complex currently consists of one 70-m diameter station, one 34-m high efficiency station and two or more 34-m beam waveguide (BWG) stations.

Goldstone's DSS-25, mentioned above, is a 34-m BWG antenna (shown in Fig. 6's upper panel) and is the primary station for Juno Gravity Science. A series of mirrors reflect the microwave energy collected by the main reflector and directed by a subreflector into the base of the antenna, referred to as the pedestal room, where transmitting and receiving equipment are placed. Multiple frequencies are directed to and from differing transmitters and receivers through the use of dichroic plates. DSS-25 is capable of receiving X-band and Ka-band signals simultaneously and currently the only station capable of transmitting the same two bands simultaneously. A new Ka-band transmitter was installed for Juno in 2015 to replace an older transmitter from the early Cassini cruise era. Co-located alongside DSS-25 are two Advanced Media Calibration units to provide high-precision corrections for the delay on the signal path caused by water vapor content in Earth's atmosphere (see Keihm et al. 2004 for methodology of water vapor calibration).

4.1 Transmitters

The X-band and Ka-band transmitters at DSS-25 utilize a frequency reference from the complex's hydrogen maser clock, the heart of the Frequency and Timing Subsystem (FTS). The transmitter-exciter subsystem (ETX) generates a frequency profile to forward-compensate for the predicted one-way Doppler shift, and optionally encode commands and ranging at X-band. The forward Doppler compensation ensures the spacecraft transponders appear to receive a near-constant frequency, which reduced the stress on the transponders. The frequency profile is a piecewise linear function over time referred to as a ramp. The two frequencies are amplified by the transmitter subsystems.

The X-band transmitter utilizes a klystron amplifier to provide up to 20 kW of output RF power, typically set to 18 kW for Juno. The upgraded Ka-band transmitter consists of two Applied Systems Engineering 277Ka Traveling Wave Tube (TWT) amplifiers at 200 W of RF power output each for a combined power output of 300 W. It is installed on top of an electronically-controlled, movable table that moves the transmitter relative to a mirror to direct the microwave energy out to the main reflector. This allows the uplink Ka-band narrow beam to be pointed ahead of the downlink Ka-band beam to correct for the relative motion of the spacecraft. This aberration correction is necessary because Juno moves up to ~ 28 millidegrees in the plane of the sky during the time it takes the signal to travel from the station to the spacecraft and back (the round-trip light time). This is outside DSS-25's Ka-band beamwidth of ~ 16 millidegrees, thus without the aberration correction, the main beam of the uplink would miss the spacecraft entirely.

4.2 Station Front End

A station's front-end refers to the microwave subsystem and the fixed first stage of the receiving down-conversion process. The primary component of the microwave subsystem is a low-noise amplifier (LNA). For distant spacecraft, the received signal is very weak due to the inverse square loss over Solar System scale distances and requires optimized amplification.

Fig. 6 *Upper panel* is DSS-25, a 34-m diameter station at NASA's Deep Space Network, Goldstone, California, capable of Ka-band uplink and downlink. In the *drawn blue circle* is the Advanced Water Vapor Radiometer (AWVR) showing relative location and size to the DSN station. The *middle panel* shows a close-up of the AWVR showing relative size to personnel. The *lowest panel* shows the two AWVRs and their Microwave Temperature Profilers (MTP); mounted on the right concrete pad are the surface meteorology packages and wind sensors

Two methods can be used, either a maser (microwave amplification by stimulated emission of radiation) or a high electron mobility transistor (HEMT). At DSS-25, the primary X-band LNA is a Traveling-Wave Maser (XTWM), with an X-band HEMT available as a backup. The Ka-band LNA is a HEMT.

The first stage of the receiver provides a fixed down-conversion from the received RF to an IF, also driven by the FTS highly stable hydrogen maser clock. At X-band, the fixed local oscillator (LO) is at 8.1 GHz and outputs at $\sim$ 300 MHz IF. The Ka-band local oscillator is at 31.7 GHz and its output is at $\sim$ 300 MHz IF. The IF signals are sent via fiber-optic lines from the station to a signal processing center a few kilometers away, a distance that the signal travels in $\sim$ 7.7 microseconds without degrading the gravity science data accuracy.

4.3 Receivers

The DSN utilizes two types of receivers: closed-loop and open-loop receivers. The Juno Gravity Science investigation utilizes both simultaneously. The closed-loop tracking receiver, referred to as the Block V Receiver (BVR), locates the carrier of the incoming signal via an initial fast-Fourier transform (FFT) acquisition software before locking onto it via a phase-locked loop (PLL). The loop tracks the phase of the downlink carrier to produce a time profile of the received phase, frequency and amplitude. In addition to carrier tracking, the BVR also provides subcarrier tracking and telemetry extraction at X-band.

An independent open-loop receiver (designed for Radio Science and VLBI experiments) performs an additional down-conversion to baseband and records the incoming signal in a pre-selected bandwidth without a lock-function. It uses a prediction file of the signal frequency profile generated in advance of the track based on the known trajectory of the spacecraft to tune a numerically controlled oscillator in the down-converter that compensates for the known Doppler effects. The open-loop receiver records In-phase and Quadrature (I and Q) samples of the voltage for additional processing by the user after the tracking pass. Due to the flexibility provided by the open-loop receiver, it allows the Doppler frequency to be extracted with greater accuracy than the closed-loop receiver.

4.4 Antenna Pointing

Accurate pointing of the DSN antenna is required in order to optimize the power of the received signals, which are weak and have narrow beamwidth as described above (narrower for higher frequencies). The location of the spacecraft, which is the signal source, is known from up-to-date navigation solutions and advanced predictions. Two techniques are used to optimize the antenna pointing, conical scanning (conscan) at X-band and monopulse at Ka-band.

The antenna is scanned conically around the expected direction of the X-band signal source in the plane of the sky. As the signal deviates from the optimum source, a receiver algorithm computes the location of the highest signal level and points the antenna towards it. This antenna pointing calibration process is optionally carried out at the beginning of the pass or after spacecraft maneuvers that can change knowledge from previous predictions. Due to its disruptive impact on the phase of the signal, it is not carried out during the actual Gravity Science observations.

Similarly, for Ka-band signals, which are narrower in beamwidth, a system called monopulse is exercised to optimize the pointing (Gudim et al. 1999). This technique compares the phase and gain of the nominal Ka-band downlink with an “error channel” in a

second receiver to determine elevation and cross-elevation corrections to the antenna pointing at the millidegree level. Periodic calibrations using a spacecraft signal are exercised during dedicated tracks to determine the required phase correction in advance of the Gravity Science observations. This is carried out by commanding the antenna to off-point by a few millidegrees; the monopulse system generates the needed correction and the error between the monopulse correction and the commanded off-point angle determines the phase value to be applied during the Gravity Science tracks. Unlike conscan at X-band, monopulse is enabled throughout the science observations at Ka-band to optimize the antenna pointing.

4.5 Media Calibration

Two Advanced Media Calibration (AMC) units are located adjacent to DSS-25 to provide a precise correction to the effect of the troposphere on the radio-metric data, as shown in Fig. 6. This system consists of several instruments. The Advanced Water Vapor Radiometer (AWVR) is the key instrument and it measures the water content along the line-of-sight at the 22.2, 23.8 and 34.1 GHz spectral lines. A Microwave Temperature Profiler (MTP) measures the atmospheric temperature along the line-of-sight. Both the AWVR and MTP co-point in the same direction as DSS-25 during the science observations; this pointing ability makes the system advanced relative to standard stationary water-vapor radiometers near other stations. A surface meteorology package and wind sensors provide those conditions at the antenna and include surface pressure, humidity, temperature, wind speed and wind direction. The observables from each instrument are statistically combined to compute a troposphere path delay correction applied in the data post-processing stage to the Gravity Science observables. The accuracy of the Juno gravity measurements will usually be limited by the accuracy of the AWVR calibration. The AWVR calibration errors occur from the measurements and models of the water brightness (see Niell et al. 2001) and from the offset and difference in beamwidth of the AWVR beam from the DSS-25 beam (see Linfield and Wilcox 2001).

5 Expected Measurement Accuracy

The accuracy of Doppler measurements using planetary spacecraft have been studied most extensively for the Cassini mission (a Doppler error budget is detailed in Asmar et al. 2005). Sources of noise include effects from the instrument itself and from fluctuations in the index of refraction in the signal path between the spacecraft and the DSN tracking station. Instrumental effects include instability of the DSN timing system, errors in the frequency tracking loops at the spacecraft, antenna mechanical vibration, and noise due to the finite signal-to-noise ratio of the received radio signals. For Cassini and Juno, these effects are smaller than the errors in calibration of fluctuations in the troposphere, with the possible exception of random motions of the DSN tracking antenna that are difficult to separate from fluctuations in the troposphere.

The Doppler accuracy can be characterized by the fractional frequency stability using the Allan deviation (Barnes et al. 1971). The average performance achieved from Cassini radio science was Allan deviation of 3×10^{-15} for averaging time of 1000 s. These measurements were predominately made at night when fluctuations due to the troposphere are generally smaller than for daytime. The Juno design requirement is for Allan deviation of 6×10^{-15} for averaging time of 1000 s over different times of day.

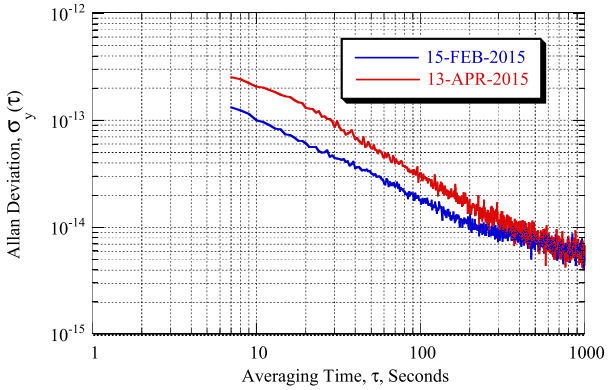

Fig. 7 Doppler measurement accuracy of the Juno radio system measured on two separate days during cruise prior to arrival at Jupiter, with Allan deviation σ_y as a function of averaging time τ

Figure 7 shows plots of Juno Doppler measurement accuracy taken on two separate days during cruise prior to arrival at Jupiter. The Allan deviation at averaging time of 1000 s is near the 6×10^{-15} required level. The Allan deviation at shorter times increases roughly as the inverse square-root of the averaging time τ, as expected for troposphere fluctuations. Performance at Jupiter may be slightly larger due to incomplete cancellation of the effects of charged particles in the Jovian system, particularly those trapped in the Io plasma torus (Eshleman et al. 1979).

Acknowledgements The authors thank the following colleagues for their notable contributions to the design, development, and testing of the various elements that constitute the Juno Gravity Science instrumentation. We especially appreciate the work at NASA's Jet Propulsion Laboratory of Michael Agnew, Kris Angkasa, Scott Bryant, Fouad Chiha, Manuel Franco, Gary Glass, David Hansen, Steve Keihm, Juan Ocampo, Aluizio Prata, Joseph Vacchione, and Phil Yates. We thank the Italian Space Agency and Thales Alenia Space-Italy, especially Dario Andreozzi and the entire Ka-band Translator team. We appreciate the extraordinary support of the management and staff of the Deep Space Network. This work was carried out in part at the Jet Propulsion Laboratory, California Institute of Technology under contract the National Aeronautics and Space Administration (NASA).

References

J.D. Anderson, G.W. Null, S.K. Wong, Gravity results from Pioneer 10 Doppler data. J. Geophys. Res. **79**, 3661 (1974)

S.W. Asmar, J.W. Armstrong, L. Iess, P. Tortora, Spacecraft Doppler tracking: noise budget and accuracy achievable in precision radio science observations. Radio Sci. **40**, RS2001 (2005)

J.A. Barnes, A.R. Chi, L.S. Cutler, D.J. Healey, D.B. Leeson, T.E. McGunigal, J.A. Mullen, W.L. Smith, R.L. Sydnor, R.F. Vessot, G.M. Winkler, Characterization of frequency stability. IEEE Trans. Instrum. Meas. **1001**, 105 (1971)

S.J. Bolton et al., The Juno mission. Space Sci. Rev. (2017, this issue). doi:10.1007/s11214-017-0429-6

J.K. Campbell, S.P. Synnott, Gravity field of the Jovian system from Pioneer and Voyager tracking data. Astron. J. **90**, 364 (1985)

S. Ciarcia, L. Simone, D. Gelfusa, P. Colucci, G. De Angelis, F. Argentieri, L. Iess, R. Formaro, MORE and Juno Ka-band transponder design, performance, qualification and in-flight validation, in *6th ESA International Workshop on Tracking, Telemetry and Command Systems for Space Applications ESA-ESOC*, 10–13 September 2013

V.R. Eshleman, G.L. Tyler, G.E. Wood, G.F. Lindal, J.D. Anderson, G.S. Levy, T.A. Croft, Radio science with Voyager at Jupiter: initial Voyager 2 results and a Voyager 1 measure of the Io torus. Science **206**, 959 (1979)

M.A. Gudim, W. Gawronski, W.J. Hurd, P.R. Brown, D.M. Strain, Design and performance of the monopulse pointing system of the DSN 34-meter beam-waveguide antennas, in *Telecommunications and Mission Operations Progress Report*, vol. 42-138 (1999).

W.B. Hubbard, B.A. Militzer, Preliminary Jupiter model. Astrophys. J. **820**(1), 80 (2016)
R.A. Jacobson, Jupiter satellite ephemeris file Jup230, in *NASA Navigation and Ancillary Information Facility* (2003). https://naif.jpl.nasa.gov/pub/naif/generic_kernels/spk/satellites/a_old_versions/jup230l.cmt
R.A. Jacobson, Jupiter satellite ephemeris file Jup310, in *NASA Navigation and Ancillary Information Facility* (2009). https://naif.jpl.nasa.gov/pub/naif/generic_kernels/spk/satellites/jup310.cmt
R.A. Jacobson, R. Haw, T. McElrath, P. Antreasian, A comprehensive orbit reconstruction for the Galileo prime mission in the J2000 system, in *Advances in the Astronautical Sciences*, vol. 103 (1999)
M.A. Janssen, J.E. Oswald, S.T. Brown, S. Gulkis, S.M. Levin, S.J. Bolton, M.D. Allison, S.K. Atreya, D. Gautier, A.P. Ingersoll, J.I. Lunine, G.S. Orton, T.C. Owen, P.G. Steffes, V. Adumitroaie, A. Bellotti, L.A. Jewell, C. Li, L. Li, S. Misra, F.A. Oyafuso, D. Santos-Costaz, E. Sarkissian, R. Williamson, J.K. Arballo, A. Kitiyakaral, A. Ulloa-Severino, J.C. Chen, F.W. Maiwald, A.S. Sahakian, P.J. Pingree, K.A. Lee, A.S. Mazer, R. Redick, R.E. Hodges, R.C. Hughes, G. Bedrosian, D.E. Dawson, W.A. Hatch, D.S. Russell, N.F. Chamberlain, M.S. Zawadskil, B. Khayatianl, B.R. Franklin, H.A. Conley, J.G. Kempenaar, M.S. Lool, E.T. Sunada, V. Vorperion, C.C. Wang, MWR: microwave radiometer for the Juno mission to Jupiter. Space Sci. Rev. (2017). doi:10.1007/s11214-017-0349-5
Y. Kaspi, Inferring the depth of the zonal jets on Jupiter and Saturn from odd gravity harmonics. Geophys. Res. Lett. **40**, 676 (2013)
S.J. Keihm, A. Tanner, H. Rosenberger, Measurements and calibration of tropospheric delay at Goldstone from the Cassini media calibration system, in *Interplanetary Network Progress Report*, vol. 42-158 (2004)
A.J. Kliore, J.D. Anderson, J.W. Armstrong, S.W. Asmar, C.L. Hamilton, N.J. Rappaport, H.D. Wahlquist, R. Ambrosini, F.M. Flasar, R.G. French, L. Iess, Cassini radio science. Space Sci. Rev. **115**, 1 (2004)
J. Lauf, M. Calhoun, W. Diener, J. Gonzales, A. Kirk, P. Kuhnle, B. Tucker, C. Kirby, R. Tjoelker, Clocks and timing in the NASA deep space network, in *Frequency Control Symposium and Exposition, Proceedings of the 2005 IEEE International* (2005)
R.P. Linfield, J.Z. Wilcox, Radio metric errors due to mismatch and offset between a DSN antenna beam and the beam of a troposphere calibration instrument, in *Interplanetary Network Progress Report*, vol. 42-114 (2001)
G. Mariotti, P. Tortora, Experimental validation of a dual uplink multifrequency dispersive noise calibration scheme for Deep Space tracking. Radio Sci. **48**, 111 (2013)
Y. Miguel, T. Guillot, L. Fayon, Jupiter internal structure: the effect of different equations of state. Astron. Astrophys. **596**, A114 (2016)
T.D. Moyer, *Formulation for Observed and Computed Values of Deep Space Network Data Types for Navigation*. DESCANSO Monograph, vol. 2 (2000)
R. Mukai, D. Hansen, A. Mittskus, J. Taylor, M. Danos, *Juno Telecommunications*. NASA DESCANSO Design and Performance Summary Series (2012)
N. Nettelmann, A. Becker, B. Holst, R. Redmer, Jupiter models with improved hydrogen EOS (H-REOS.2). Astrophys. J. **750**, A52 (2012)
A.E. Niell, A.J. Coster, F.S. Solheim, V.B. Mendes, P.C. Toor, R.B. Langley, C.A. Upham, Comparison of measurements of atmospheric wet delay by radiosonde, water vapor radiometer, GPS, and VLBI. J. Atmos. Ocean. Technol. **18**, 830 (2001)
G.W. Null, J.D. Anderson, S.K. Wong, Gravity field of Jupiter from Pioneer 11 tracking data. Science **188**, 476 (1975)
P.F. Thompson, M. Abrahamson, S. Ardalan, J. Bordi, Reconstruction of Earth flyby by the Juno spacecraft, in *AAS-435* (2014)
J.D. Vacchione, R.C. Kruid, A. Prata, L.R. Amaro, A.P. Mittskus, Telecommunications antennas for the Juno Mission to Jupiter, in *IEEE Aerospace Conference* (2012)
S.M. Wahl, W.B. Hubbard, B. Militzer, Tidal response of preliminary Jupiter model. Astrophys. J. **831**, 14 (2016)